View metadata, citation and similar papers at core.ac.uk

brought to you by CORE

provided by University of Bath Research Portal

Citation for published version:
Muttakin, I, Wondrak, T & Soleimani, M 2020, 'Magnetic Induction Tomography Sensors for Quantitative Visualisation of Liquid Metal Flow Shape', *IEEE Sensors Letters*, vol. 4, no. 7, 6001204. https://doi.org/10.1109/LSENS.2020.3000292

DOI:
10.1109/LSENS.2020.3000292

Publication date:
2020

Document Version
Peer reviewed version

Link to publication

© 2020 IEEE. Personal use of this material is permitted. Permission from IEEE must be obtained for all other users, including reprinting/ republishing this material for advertising or promotional purposes, creating new collective works for resale or redistribution to servers or lists, or reuse of any copyrighted components of this work in other works.

University of Bath

Alternative formats
If you require this document in an alternative format, please contact:
openaccess@bath.ac.uk

General rights
Copyright and moral rights for the publications made accessible in the public portal are retained by the authors and/or other copyright owners and it is a condition of accessing publications that users recognise and abide by the legal requirements associated with these rights.

Take down policy
If you believe that this document breaches copyright please contact us providing details, and we will remove access to the work immediately and investigate your claim.

Download date: 17. Jul. 2021

Sensor Applications

Magnetic Induction Tomography Sensors for Quantitative Visualisation of Liquid Metal Flow Shape

Imamul Muttakin[1*], Thomas Wondrak[2], and Manuchehr Soleimani[1]

[1] Department of Electronic & Electrical Engineering, University of Bath, United Kingdom
[2] Institute of Fluid Dynamics, Helmholtz-Zentrum Dresden-Rossendorf, Germany
[*] Member, IEEE

Manuscript received June 7, 2017; revised June 21, 2017; accepted July 6, 2017. Date of publication July 12, 2017; date of current version July 12, 2017.

Abstract—The work proposes magnetic induction tomography (MIT) sensors for liquid metal visualisation. Design aspect and performance evaluation, which by far were overlooked, are presented to quantify the shape of conductive substance against non-conductive region. Portable MIT sensors have been constructed and tested on GaInSn in the submerged entry nozzle (SEN) model. Reconstruction result shows applicability for liquid metal imaging. This feature meets the need to observe flow regime and phase distribution of steel in continuous casting. There are challenging flow regimes that can not yet fully be recovered, which are also investigated here.

Index Terms—tomography, continuous casting, MIT, liquid metal, GaInSn.

I. INTRODUCTION

In continuous casting within the steel manufacturing process, flow regime, phase distribution, as well as gas inclusion in the submerged entry nozzle (SEN) are very important phenomena related to steel quality. Electromagnetic induction method is arguably the most applicable technique, since optical or nuclear means are not feasible for a real caster. Sensors have been developed and tested for liquid steel two-phase flow measurements [1] [2]. Nevertheless, the need of a combined tomographic imaging approach arises because there is no unique measurement technique that can resolve the outer interface and bubbles in the liquid metal bulk with sufficient accuracy.

Magnetic induction tomography (MIT) is able to reconstruct the conductivity distribution in one cross-section of the SEN, and thereby to distinguish between liquid metal and argon gas in case of a two-phase flow. Previous researches [3] [4] have satisfactorily presented qualitative result on measurement and/or imaging liquid metal distribution in the vessel. In order to incorporate the apparatus onto a regulated process, a quantified information on both metal shape and inclusion, as well as a precise, fast measurement with a real-time reconstruction is required.

Sensors for monitoring the steel flow are needed, which are rugged, inherently safe and capable of visualising flow and clogging circumstances. As a real-world insight for interested readers, operation practices for steel cleanliness were reviewed in [5]. This work explores MIT sensors in a portable construction fitted for SEN model. The aim is to develop a measurement system which can be integrated into a control loop.

II. ELECTROMAGNETIC TOMOGRAPHY

Method for generating cross-sectional image utilizing a low-intensity electromagnetic field as excitation energy has been developed for the past three decades. It is capable of examining the electrical properties of the object such as conductivity and permeability. Owing to contact-less non-invasive non-intrusive low-cost system and fast imaging process, it has been rigorously appraised for various applications, from industrial to medical.

Magnetostatics approach is established to extract the conductivity and/or permeability in the sensing area. It uses eddy current field measurement to distinguish the object in contrast with the background field. MIT principle is depicted in Fig. 1, where a coil is excited by

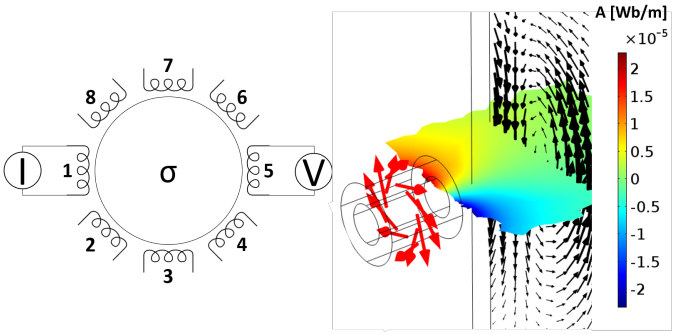

Fig. 1. MIT measurement concept.

current I (red arrows), while the other coil is induced by voltage V as a result of $\mathbf{A}$ field (surface plot) in the region with the distribution of conductivity σ and eddy current (black arrows).

Magnetic vector potential is defined to form the given governing equation of eddy current, neglecting electric field, displacement current, and propagation effects [6]:

$$\nabla \times \frac{1}{\mu} \nabla \times \mathbf{A} + j\omega\sigma\mathbf{A} = \mathbf{J}_s \tag{1}$$

where μ is permeability, $\mathbf{A}$ is magnetic vector potential, ω is angular frequency of the current in the coil, σ is electrical conductivity, and $\mathbf{J}_s$ is excitation current density.

Corresponding author: I. Muttakin (e-mail: nospam@nospam.org).
(For the real e-mail address, see https://people.bath.ac.uk/im463/).
Associate Editor: Alan Smithee.
Digital Object Identifier 10.1109/LSENS.2017.0000000

1949-307X © 2017 IEEE. Personal use is permitted, but republication/redistribution requires IEEE permission.
See http://www.ieee.org/publications_standards/publications/rights/index.html for more information.

The system is implemented as procedures: signal source excites a coil while the rest being induced in accordance with field interaction in the sensing area. Multiplexers are used for selecting excitation and detection electrodes as measurement sequences. Data acquisition is conditioning and interfacing the result to a computer where it will be post-processed reconstructing tomographic image. Thus, tomographic data are formed as arrays of sensors' measurement combination. In the case of 8 sensors, each of which can act as either exciter or detector, one frame (a complete set of 'projection') consists of (C_2^8) 28 readings.

MIT sensors' output are induced voltage (2) on detector coil (through which virtual unit current density J_0 flows) due to vector ($\mathbf{A}$) magnetic field generated by exciter coil and secondary field from eddy current which occurs on conductive object in the sensing area [7]. Therefore MIT data reveals conductive against non-conductive regime. For time-difference imaging technique, the changes versus background reference are taken into account.

$$V = -j\omega \int \mathbf{A} \cdot J_0 dl \tag{2}$$

The general form of the sensitivity formula for excitation-detection pairs (e.g. coil-1 and coil-5 in Fig. 1) is [8]

$$\int_\Gamma \delta\mathbf{E}_1 \times \mathbf{H}_5 \cdot \mathbf{n} ds = \int_\Omega -j\omega\delta\mu\mathbf{H}_1 \cdot \mathbf{H}_5 + (\delta\sigma + j\omega\delta\varepsilon)\mathbf{E}_1 \cdot \mathbf{E}_5 dv \tag{3}$$

where the left-hand-side represents excitation and detection by surface integral on surface Γ; while the right-hand-side is the volume integral over the perturbed region Ω. The magnetic and electric fields when sensor 1 is excited are $\mathbf{H}_1$ and $\mathbf{E}_1$; whereas $\mathbf{H}_5$ and $\mathbf{E}_5$ are the magnetic and electric fields when sensor 5 is excited. Therefore, a relationship between the change of detection voltage and conductivity change at eddy current region can be derived from dot product of electric fields [9]. In this work, the space Ω is discretised onto elements in two-dimensional 50×50 pixel along X and Y axes.

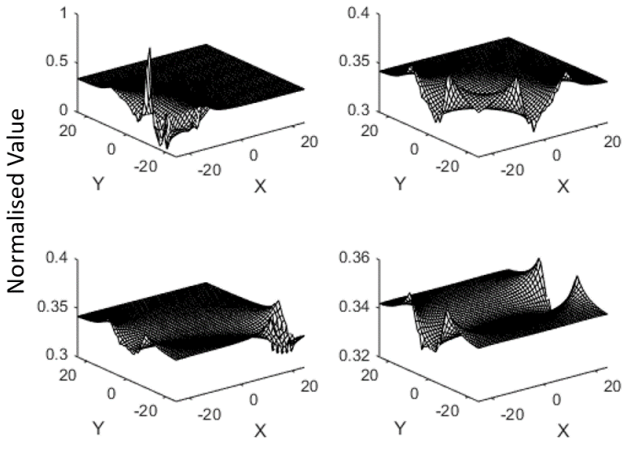

Fig. 2. Sensitivity map.

Fig. 2 illustrates a computed sensitivity map for coil pairs in adjacent (top-left), orthogonal (top-right), near-opposite (bottom-left), and opposite (bottom-right) positions. These four maps are the basis which can be rotated to form a full combination sensitivity matrix. They are plotted relative to the adjacent map's value, and reveals high-sensitive regions near the boundary. This will affect the reconstruction result (provided later in Section IV).

III. LIQUID METAL MEASUREMENT

The liquid metal used in experiments is a eutectic alloy of gallium indium tin (GaInSn) which has a liquid phase in room temperature. Essential material property of GaInSn in term of electrical conductivity is 3.2 MS/m [10] which is intended for electromagnetic sensors.

A. Continuous Casting Model

A small-scale facility for continuous casting model was constructed at Helmholtz-Zentrum Dresden-Rossendorf (HZDR) namely Mini-LIMMCAST (Liquid Metal Model for Continuous Casting) for experimental program on quantitative flow measurement of liquid metal [11]. The ultimate objective of this research is to control the process utilising data and/or image from tomographic sensors, the scheme of which is sketched in Fig. 3.

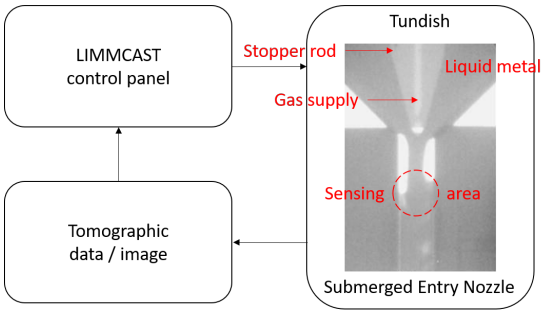

Fig. 3. Mini-LIMMCAST at HZDR.

The part of interest for this work, in particular, is SEN in which liquid metal is flowing from tundish to mould (x-ray captured Fig. 3 right) [12]. Imaging area is focused on a section where the two-phase distribution of liquid metal and gas are present. In the Mini-LIMMCAST experiment, liquid metal velocity in the SEN is approximately $1 - 2\ m/s$ within which injected gas bubble size is estimated between $2\ mm - 5\ mm$ in diameter. Therefore, the sensor should be sensitive to approximately 2.5% – 20% area fraction of inclusion. As for the actual implementation, acquisition rate around 100 frame-per-second is required.

B. Sensor Design

The sensor's construction is seen in Fig. 4. An individual part (left figure) is ferrite-cored multi-layer coil. Eight of them are assembled evenly (45^o axisymmetric) into a plastic housing (right figure) to form a circular array of coils circumventing the sensing space. Besides as a fitting for SEN pipe, the housing can be exploited for shielding to increase the sensors' sensitivity and reject any external interference. Structural details of the sensor are given in Table. 1

In terms of measurement, the sensitivity of a ferrite-cored induction coil sensor is defined as the amount of induced voltage V per unit field H at operating frequency f, and can be calculated [13]:

$$\frac{V}{H} \approx 0.9 \times 10^{-5} \cdot f \cdot \frac{l^3}{d_w^2} \cdot d_i \cdot \frac{1}{ln(2l/d_i) - 1} \tag{4}$$

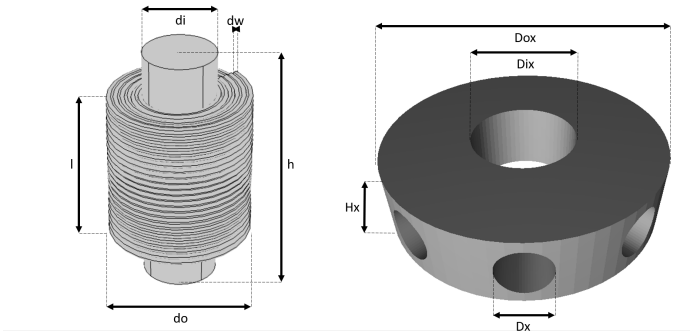

Fig. 4. Sensor design.

TABLE 1. Sensor parameter

Parameter	Symbol	Value
Wire diameter	dw	32 AWG
Coil inner diameter	di	2.5 mm
Coil outer diameter	do	5 mm
Coil length	l	5 mm
Core height	h	8 mm
Case inner diameter	Dix	15 mm
Case outer diameter	Dox	40 mm
Case slot diameter	Dx	7 mm
Case height	Hx	10 mm

From simulation (following method in [14]), it is evaluated that resultant magnetic field H (air background) on the edge of receiving coil ($x = 7.5\ mm$) is 1.2155 (A/m) at 1 kHz. The typical MIT receiving circuitry has resolution down to 0.125 mV, using combination of analog-to-digital conversion and programmable gain amplifier [15]; while expected signal level for detection is 0.216 mV. Therefore, the designed sensor is expected to response towards the exposing field and generate sufficient level for common measuring hardware resolution.

C. Measurement Setup

The sensors are connected to MIT hardware system developed in University of Bath [16]. The scheme is shown in Fig. 5 (left) where 8-coils are formed surrounding SEN pipe made of PMMA with diameter of 15 mm and 2.5 mm wall thickness. Fig. 5 (right) shows a setup in which a contained liquid metal strand (diameter of 7 mm) is placed in the centre of SEN pipe while MIT measurements are taken. Operating frequency of 130 Hz (penetrating 24 mm depth through GaInSn) is chosen. This particular operating frequency was also successfully applied in previous work on steel imaging [17].

IV. VISUALISATION RESULT

Conductivity distribution of material is obtained from measured data using image reconstruction technique. Induced voltage values are taken as a function conceived by electrical conductivity. Matrix equation can be described [2]:

$$\mathbf{V} = \mathbf{SK} \tag{5}$$

where $\mathbf{V}$ is voltage measurement data, $\mathbf{S}$ is sensitivity map (representing responses of each sensors' section to particular measurement) also called Jacobian, and $\mathbf{K}$ is conductivity values. Given the $\mathbf{V}$ from

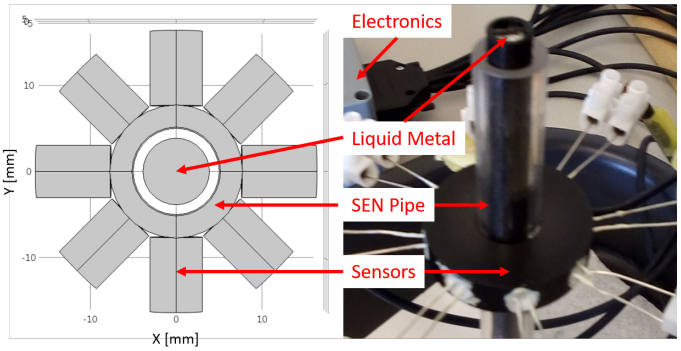

Fig. 5. Experiment for liquid metal in SEN tube.

experiment and the $\mathbf{S}$ formulated from prior forward computation, the pixelated conductivity $\mathbf{K}$ can be estimated,

$$\mathbf{K} \approx \mathbf{S}^{+}\mathbf{V}. \tag{6}$$

The $\mathbf{S}^{+}$ could be in form of $(\mathbf{S}^{T}\mathbf{S} + \lambda\mathbf{R})^{-1}\mathbf{S}^{T}$ where $\mathbf{R}$ and λ are the regularisation matrix and regularisation parameter (order of 10^{-12}) respectively. This method [18] to some extent is adequate for image observation, especially with high conductivity contrast and centralised distribution.

Since MIT will be applied to determine two-phase distribution of liquid metal and gas inside the SEN, tests with different filling regimes have been observed. Fig. 6 (top of each section) shows several metal flow scenarios (assumed from Fig. 3) molded as 3-d printed containers (PLA material) and measured by the sensor. The images are generated against either empty-air or full-metal background reference. Normalisation of low perturbation against high background was also explained in [19].

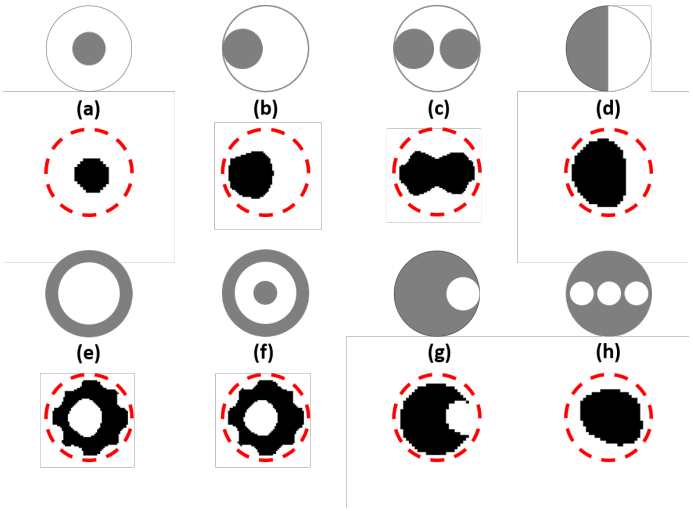

Fig. 6. MIT imaging for metal flow scenarios in SEN.

The reconstructed images are shown in the bottom of respective sections in Fig. 6. Red dashed-line indicates the actual boundary of the containers. From left to right, top-bottom, cross-sectional image is depicted for central-stream occupying 15% of total area (a), side-stream 20% (b), split-streams 20% each (c), stratified 50% (d), annular 50% (e), annular –wispy– with internal strand 7.5% (f), void-side 20% (g), and bubbly (three voids) each of which has area

fraction 7.5% (h). Taking fully-filled metal as threshold value, there are distinct regimes of conductive (metal) and non-conductive (gas) phase, except for difficult cases where the sensitivity is weak in the centre region. Still, the measurements have a good consistency across a hundred data for each case (12 seconds measurement time) with an average signal-to-noise ratio (SNR) of 62.93 dB.

Evaluating the performance of MIT sensors in terms of imaging result, correlation coefficient (CC) and relative error (RE) are used, as commonly adopted for electromagnetic tomography [20],

$$CC = \frac{\sum_{i=1}^{N}(\hat{g}_i - \bar{\hat{g}})(g_i - \bar{g})}{\sqrt{\sum_{i=1}^{N}(\hat{g}_i - \bar{\hat{g}})^2 \sum_{i=1}^{N}(g_i - \bar{g})^2}} \tag{7}$$

$$RE = \frac{||\hat{G} - G||}{||G||} \tag{8}$$

where $\hat{g}_i$ and $\bar{\hat{g}}$ are ith element and average of the reconstructed image; while g_i and $\bar{g}$ are ith element and average of the actual distribution respectively. On the other hand, $\hat{G}$ is overall reconstructed image; whereas G is overall actual distribution.

TABLE 2. Imaging evaluation

Shape	CC	RE
Central stream (a)	0.8888	0.2787
Side stream (b)	0.9063	0.2048
Split streams (c)	0.8693	0.2213
Stratified (d)	0.8928	0.2979
Annular (e)	0.4284	0.7472
Wispy annular (f)	0.3506	0.7012
Void side (g)	0.9015	0.3666
Bubbly (h)	0.8002	0.5702

Table. 2 lists imaging evaluation for different cases. If the image and the actual shape are directly correlated, the value of CC will be approaching unity; whereas if the image and the actual shape are identical, the value of RE will be zero. Central-stream, side-streams and stratified cases are reconstructed quite well. The void-side case still has a decent confirmation. For internal recovery such as wispy-annular and bubbly cases, the distribution are failed to be seen, as reflected by correlations below 0.5 and higher error values. The nature of reconstruction algorithm and the simplified subtraction/thresholding method are among reasons why image generation for some cases are less satisfactory and having artifacts at different regions depending on the object's distribution. In the future Mini-LIMMCAST experiment, metal strand and/or bubble size around 5 mm in the SEN would be the detection limit of the designed sensors.

V. CONCLUSION

Electromagnetic sensors have been designed and tested to visualise the static liquid metal profile inside the SEN model for steel casting. Quantitative evaluations are provided for several flow scenarios, both outer shapes and internal recoveries. Flow shapes are satisfactorily reconstructed with good correlations and low imaging errors. However, inner structures are difficult to obtain, especially for small-centralised inclusion or distributed bubbles. Future directions would be to use spectroscopy methods for accurately revealing internal distributions, frame rate improvement, and time-dependent behaviour. The proposed sensor has the potential to be implemented for Mini-LIMMCAST facility in an integrated control experiment.

REFERENCES

[1] R. Binns, A. R. A. Lyons, A. J. Peyton, W. D. N. Pritchard, "Imaging molten steel flow profiles," Meas. Sci. Technol., vol. 12, pp. 1132-1138, 2001.

[2] X. Ma, A. J. Peyton, R. Binns and S. R. Higson, "Electromagnetic techniques for imaging the cross-section distribution of molten steel flow in the continuous casting nozzle," in IEEE Sensors Journal, vol. 5, no. 2, pp. 224–232, April 2005.

[3] N. Terzija, W. Yin, G. Gerbeth, F. Stefani, K. Timmel, T. Wondrak, and A. Peyton, "Electromagnetic inspection of a two-phase flow of GaInSn and argon," Flow Measurement and Instrumentation, vol. 22, no. 1, pp. 10–16, Mar. 2011.

[4] T. Wondrak et al., "Combined electromagnetic tomography for determining two-phase flow characteristics in the submerged entry nozzle and in the mold of a continuous casting model", Metall. Mater. Trans. B, vol. 42, no. 6, pp. 1201-1210, 2011.

[5] L. Zhang and B. G. Thomas, "State of the Art in Evaluation and Control of Steel Cleanliness," ISIJ International, vol. 43, no. 3, pp. 271–291, 2003

[6] A. J. Peyton, "Electromagnetic induction tomography," in Industrial Tomography: Systems and Applications, M. Wang, Ed. Woodhead Publishing, 2015, pp. 61—107.

[7] C. Ktistis, D. W. Armitage and A. J. Peyton, "Calculation of the forward problem for absolute image reconstruction in MIT," Physiol. Meas., vol. 29, pp. S455-S464, 2008.

[8] D. N. Dyck, D. A. Lowther and E. M. Freeman, "A method of computing the sensitivity of electromagnetic quantities to changes in materials and sources," in IEEE Transactions on Magnetics, vol. 30, no. 5, pp. 3415–3418, Sept. 1994.

[9] M. Soleimani and W. R. B. Lionheart, "Image reconstruction in three-dimensional magnetostatic permeability tomography," in IEEE Transactions on Magnetics, vol. 41, no. 4, pp. 1274–1279, April 2005.

[10] Y. Plevachuk, V. Sklyarchuk, S. Eckert, G. Gerbeth, and R. Novakovic, "Thermophysical Properties of the Liquid Ga–In–Sn Eutectic Alloy," J. Chem. Eng. Data, vol. 59, no. 3, pp. 757—763, Mar. 2014.

[11] K. Timmel, S. Eckert, G. Gerbeth, F. Stefani, and T. Wondrak, "Experimental Modeling of the Continuous Casting Process of Steel Using Low Melting Point Metal Alloys - the LIMMCAST Program," ISIJ Int., vol. 50, no. 8, pp. 1134–1141, 2010.

[12] K. Timmel, N. Shevchenko, M. Roder, M. Anderhuber, P. Gardin, S. Eckert, and G. Gerbeth, "Visualization of Liquid Metal Two-phase Flows in a Physical Model of the Continuous Casting Process of Steel," Metall and Materi Trans B, vol. 46, no. 2, pp. 700–710, Apr. 2015.

[13] S. Tumanski, "Induction coil sensors—a review," Meas. Sci. Technol., vol. 18, no. 3, pp. R31—R46, 2007.

[14] F. N. Adiputri, E. N. Prasetiani, Rohmadi, A. Saputra, I. Muttakin and W. P. Taruno, "Simulation of Magnetic Induction Tomography Sensor with 8-Coils Solenoid and Planar," 2017 5th International Conference on Instrumentation, Communications, Information Technology, and Biomedical Engineering (ICICI-BME), Bandung, 2017, pp. 1–5.

[15] M. Al-Hawari, A. I. Aulia, A. Rudin, Rohmadi, I. Muttakin and W. P. Taruno, "Receiver Circuit Design for Signal Conditioning in Magnetic Induction Tomography System," 2017 5th International Conference on Instrumentation, Communications, Information Technology, and Biomedical Engineering (ICICI-BME), Bandung, 2017, pp. 1-6.

[16] L. Ma and M. Soleimani, "Magnetic Induction Spectroscopy for Permeability Imaging," Sci. Rep., vol. 8, no. 1, p. 7025, 2018.

[17] M. Soleimani, F. Li, S. Spagnul, J. Palacios, J. I. Barbero, T. Gutiérrez and A. Viotto, "In situ steel solidification imaging in continuous casting using magnetic induction tomography," Meas. Sci. Technol., vol. 31, no. 6, p. 065401, 2020.

[18] H.-Y. Wei and M. Soleimani, "Two-Phase Low Conductivity Flow Imaging Using Magnetic Induction Tomography," Progress In Electromagnetics Research, Vol. 131, 99–115, 2012.

[19] S. Chowdhury, Q. M. Marashdeh and F. L. Teixeira, "Inverse Normalization Method for Cross-Sectional Imaging and Velocimetry of Two-Phase Flows Based on Electrical Capacitance Tomography," in IEEE Sensors Letters, vol. 2, no. 1, pp. 1-4, March 2018, Art no. 1500704.

[20] C. G. Xie, S. M. Huang, C. P. Lenn, A. L. Stott and M. S. Beck, "Experimental evaluation of capacitance tomographic flow imaging systems using physical models," in IEE Proceedings - Circuits, Devices and Systems, vol. 141, no. 5, pp. 357–368, Oct. 1994.